IEEE Photonics Journal
An IEEE Photonics Society Publication

Open Access

High Sensitivity Integrated Visible to Mid-Infrared Nonlinear Plasmonic Sensor

Volume 9, Number 4, August 2017

F. Che
S. A. Ponomarenko
M. Cada
N. Nguyen-Huu

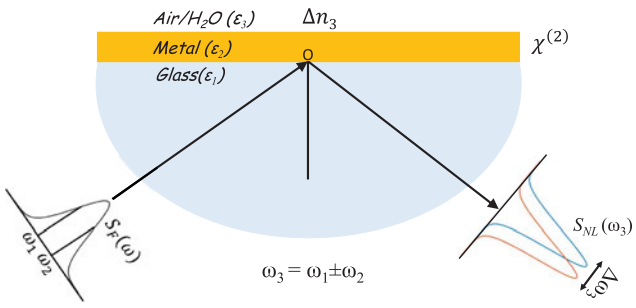

DOI: 10.1109/JPHOT.2017.2709808
1943-0655 © 2017 IEEE

High Sensitivity Integrated Visible to Mid-Infrared Nonlinear Plasmonic Sensor

F. Che,[1] S. A. Ponomarenko,[1] M. Cada,[1] and N. Nguyen-Huu[2]

[1]Department of Electrical and Computer Engineering, Dalhousie University, Halifax, NS B3H 4R2, Canada
[2]Metamaterials Technologies Inc, Technology and Innovation Centre, Dartmouth, NS B2Y 4M9, Canada

DOI:10.1109/JPHOT.2017.2709808

Manuscript received April 8, 2017; revised May 14, 2017; accepted May 23, 2017. Date of publication June 7, 2017; date of current version June 21, 2017. Corresponding author: F. Che (e-mail: franklin.che@dal.ca).

Abstract: We propose a Kretschmann-based nonlinear plasmonic sensor with a gold thin film deposited on a glass prism. Visible and mid-infrared signals are generated in this configuration through the nonlinear processes of sum- and difference-frequency generation, respectively. The calculated maximum sensitivity and figure of merit of our sum-frequency-based sensor is an order of magnitude higher than that of a traditional Kretschmann-based sensor in the visible range. Our difference-frequency-based sensor has a maximum sensitivity of 1.0×10^6 nm/RIU in air at 4.29 μm, which is three orders of magnitude higher than that of existing devices in the mid-infrared range, with its maximum figure of merit almost two orders of magnitude higher than the alternatives. By comparison, the calculated sensitivity for operation in water for both sum- and difference-frequency is about half that in air. We, thus, demonstrate significant gains in the sensitivity of the well-known Kretschmann-based plasmonic sensor over a wide wavelength range, without modifying the physical sensor, but by exploiting and simply taping the nonlinear optical properties of the system.

Index Terms: Plasmonics, nonlinear, surface, biosensors.

1. Introduction

In the past decade or so we have witnessed rapid development in the field of plasmonics which exploits collective oscillations of conduction electrons in metals [1], [2]. These oscillations are also known as surface plasmon resonance (SPR), with the position and intensity of the SPR strongly affected by the type of conductor and dielectric properties of the surrounding environment [2], [3]. This has led to the development of a variety of sensors with applications to biochemical and environmental sensing [4]–[8].

The most common SPR sensor configuration is based on the Kretschmann coupling geometry, whereby a metal thin film is deposited on a glass prism [9]. Changes in the refractive index of the dielectric on the metal film can be matched to either angular or spectral changes in the reflected linear fundamental wave (FW) from the sensor. Despite its simplicity, the Kretschmann-based sensor has limited sensitivity [10], which has led to a move towards other plasmonic sensors such as local surface plasmon (LSP) [11], grating-coupled [12], optical fibre [13] and composite [14] sensors that offer greater sensitivity.

Most of the plasmonic sensors mentioned above work within the framework of linear plasmonics, where there is no frequency mixing within the incident light source spectrum bandwidth. On the other

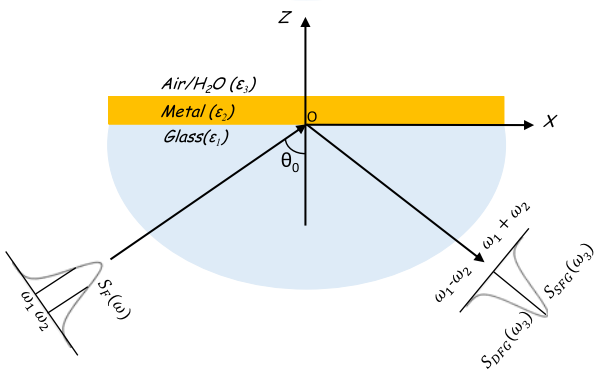

Fig. 1. Irradiation configuration.

hand, most of the research carried out in the field of nonlinear plasmonics, is geared towards the fundamental understanding of generation, modification and enhancement of harmonic frequencies [15]–[20]. However, there has been some progress made in the development of nonlinear plasmonic sensors based on the processes of second (SHG) [21], [22] and third harmonic generation [23], with most of these sensors based on LSP resonance of nanoparticles.

We have recently demonstrated [24], [25] plasmon-enhanced spectral changes in reflected sum-frequency generation (SFG) and difference-frequency generation (DFG) using the simple Kretschmann configuration. In the current study, we propose a robust, simple and highly sensitive nonlinear surface plasmon sensor operating at visible and mid-infrared (MIR) wavelengths based on the Kretschmann geometry. We demonstrate ultra high wavelength sensitivities for the proposed sensor compared to that of traditional Kretschmann plasmonic sensors [10], [26], especially at mid-infrared wavelengths, where many metals experience huge losses [27]. We also estimate the signal strength and figure of merit of the proposed sensor.

2. Kretschmann Coupling Geometry and Theoretical Background

We use the so-called Kretschmann configuration shown in Fig. 1 for our proposed sensor. Our sensor is dynamic in the sense that we use the same physical sensor over a wide wavelength range as opposed to the traditional Kretschmann sensor which operates only at optical frequencies. The conducting film is deposited on a glass prism with permittivity $\varepsilon_1 = 2.25$ and thickness d. We are using gold as the thin film of choice in this investigation due to its inertness and compatibility with biological samples. Other metals can be used for our sensor as well, depending on the sample of interest. Silver in particular has been shown to have a strong plasmonic response at visible frequencies, with very sharp resonance peaks and could be used if inertness and stability are not important for a sample under examination [10].

With the physical structure of the sensor fully defined, we then proceed to briefly outline the theory of the linear and nonlinear interaction of light incident on a metal film in this geometry. The light source is assumed to generate a highly collimated and fully spatially coherent plane wave [28]–[30]. The incident FW with a spectral amplitude $A(\omega)$ is represented by

$$\mathbf{E}_0(x, z, \omega, \theta_0) = A(\omega)\left(\frac{k_{1z}}{k_1}\mathbf{e}_x - \frac{k_x}{k_1}\mathbf{e}_z\right) e^{j(k_x x + k_{1z} z)}, \tag{1}$$

where $\mathbf{k}_1 = (k_x, 0, k_{1z})$ and $k_1 = (\omega/c)\sqrt{\varepsilon_1}$, with $\mathbf{k}_1$ expressed in terms of the incident angle θ_0 as $k_x = k_1 \sin\theta_0$ and $k_{1z} = k_1 \cos\theta_0$.

Whenever the FW is incident on the metal, it undergoes multiple reflections within the thin film. The cumulative reflected FW from the film can be calculated using the Airy summation technique

[31] and is given by

$$\mathbf{E}_r(x, z, \omega, \theta_0) = A(\omega)\left(-\frac{k_{1z}}{k_1}\mathbf{e_x} - \frac{k_x}{k_1}\mathbf{e_z}\right) \times \tilde{r}_{12}(\omega, \theta_0)e^{j(k_x x - k_{1z} z)}, \tag{2}$$

where $\tilde{r}_{12}(\omega, \theta_0)$ is the Fresnel reflection coefficient for p-polarization given by [32]

$$\tilde{r}_{12}(\omega, \theta_0) = \frac{r_{12} + r_{23}e^{j2k_{2z}d}}{1 + r_{12}r_{23}e^{j2k_{2z}d}}, \tag{3}$$

with $k_{2z} = \sqrt{k_2^2 - k_x^2}$, $k_2 = (\omega/c)\sqrt{\varepsilon_2}$; $r_{\alpha\beta}$ represents the reflection coefficient of the interface between media α and β, $(\alpha, \beta = 1, 2, 3)$.

The energy spectrum of the incident $S_0(\omega, \theta_0)$ and reflected $S_r(\omega, \theta_0)$ waves can be written as [33]

$$S_{0,r}(\omega, \theta_0) \propto \left|\mathbf{E}_{0,r}(\omega, \theta_0)\right|^2. \tag{4}$$

The incident wave excites surface polarizations at both the lower and upper interfaces of the gold film. We use the undepleted pump approximation implying that the power of the incident FW is assumed to be constant. Thus the general ith component of the sum-frequency polarization field is given by [34]

$$P_i(\mathbf{r}, \omega_3) = \varepsilon_0 \sum_{jk} \int_{-\infty}^{\infty} \frac{d\omega_1}{2\pi} \chi^{(2)}_{S,ijk}(-\omega_3; \omega_1, \omega_2) \times E_j(\mathbf{r}, \omega_1)E_k(\mathbf{r}, \omega_2), \tag{5}$$

and the difference-frequency polarization given by

$$P_i(\mathbf{r}, \omega_3) = \varepsilon_0 \sum_{jk} \int_{-\infty}^{\infty} \frac{d\omega_1}{2\pi} \chi^{(2)}_{S,ijk}(\omega_3; \omega_1, \omega_2) \times E_j(\mathbf{r}, \omega_1)E^*_k(\mathbf{r}, \omega_2). \tag{6}$$

Here $(i, j, k = x, y, z)$, ω_1 and ω_2 are the pump frequencies within the incident fundamental pulse bandwidth; $\omega_3 = \omega_1 \pm \omega_2$ represents the generated sum $(+)$ and difference $(-)$ frequencies and the asterisk $(*)$ denotes a complex conjugate. $\chi^{(2)}_{S,ijk}(\mp\omega_3; \omega_1, \omega_2)$ is the nonlinear surface susceptibility tensor of the SFG and DFG processes respectively.

We use Eq. (1), (5) and (6) to evaluate the nonlinear polarization at the lower and upper interfaces of the film. These lower and upper interface polarizations act as source currents at the nonlinear frequency, and the resulting sum- or difference-frequency field is given by

$$E_i(\mathbf{r}, \omega) = \frac{(\omega/c)^2}{\varepsilon_0} \sum_{jk} \int d\mathbf{r}' G_{ij}(\mathbf{r}, \mathbf{r}', \omega)P_j(\mathbf{r}', \omega). \tag{7}$$

Here $G_{ij}(\mathbf{r}, \mathbf{r}')$ is a dyadic Green's function [35]. The reflected sum-and difference-frequency signal spectra can then be determined from their definitions, Eq. (4). We have presented just a general outline of the theoretical formulation with the complete treatment and technical details found in [24], [25]. It should be noted that all quantities in Eq. (7) are evaluated at either the sum or difference frequency ω_3.

The proposed plasmonic sensor performance is evaluated by its sensitivity, $S(\lambda)$ and figure of merit (FOM). For our sensor, $S(\lambda)$ measures the dependence of the reflected nonlinear resonance peak position on changes in the refractive index of the dielectric environment (ε_3), while the FOM determines the measurement accuracy of the sensor by taking into account the spectral width of the reflected signal. Ideally, we want a sensor with high values of both sensitivity and FOM. The

wavelength sensitivity of a plasmonic sensor is defined as [36]

$$S(\lambda) = \frac{\Delta\lambda}{\Delta n}, \tag{8}$$

where n is the refractive index of the dielectric sample (ε_3), and λ is the peak wavelength of the reflected wave. By changing the dielectric constant of medium 3, we calculate the resultant shifts in the peak position of the nonlinear reflected spectrum and use this to determine the spectral sensitivity. The FOM is defined as [37]

$$FOM = \frac{S(\lambda)}{FWHM}, \tag{9}$$

where FWHM is the full width at half maximum of the reflectance dip (linear sensor) or peak (nonlinear sensor) spectrum. The signal to noise ratio (SNR) is sometimes used to evaluate the performance of a SPR sensor and is defined by [38]

$$SNR = \frac{\Delta\lambda}{FWHM}. \tag{10}$$

The FOM provides the same qualitative information as the SNR and thus we will limit our discussions to just the FOM in this paper. We aim to achieve high SNR or FOM values by optimizing the sensitivity of our system. Besides the sensitivity and FOM, other possible factors that affect the performance of a SPR biosensor include; noise from the optical system and readout electronics, mechanical stability of the sensor, resolution and the limit of detection [39] of the sensor which can be evaluated when the physical sensor is tested.

3. SFG-Based Sensor

For operation at visible wavelengths, we use the nonlinear process of SFG, where the incident FW is a femtosecond Gaussian laser pulse in the near infrared range. Most metals have a strong plasmonic response at frequencies in this range [40]. Spectral modulations in the reflected linear field for ultrashort pulses in the Kretschmann configuration have been reported at these frequencies [41], [42]. The plasmon-enhanced spectral modulation of the incident light when it couples into surface plasmon polaritons subsequently generates more spectral signatures in the reflected nonlinear light through nonlinear polarization.

As a demonstration, we use a 10 fs laser pulse with a peak wavelength of 1178 nm shown in Fig. 2(a) which is incident on a 50 nm thick gold film chosen for optimum resonance [43], to generate a sum-frequency field at 588.6 nm. Fig. 2(b), shows the reflected FW, with the hole in the spectrum representing the coupling of light into surface plasmon polaritons. The angle of incidence for which light couples into surface plasmon polaritons is given by [35]

$$\theta_c(\omega) = \arcsin\left[\sqrt{\frac{\varepsilon_2(\omega)\varepsilon_3(\omega)}{\varepsilon_1(\varepsilon_2(\omega)+\varepsilon_3(\omega))}}\right]. \tag{11}$$

The calculated plasmon coupling angle at the centre wavelength using Eq. (11) is $\theta = 42.30^\circ$, which corresponds well to the hole location in Fig. 2(b). The reflected sum-frequency field is shown in Fig. 2(c), with the maximum intensity corresponding to the surface plasmon coupling angle of the FW. Finally Fig. 2(d) shows the SFG spectrum normalized for each angle of incidence, to clearly show the position of SFG spectral peak close to SPR. The normalization is done by dividing the spectrum for each angle of incidence by the peak spectral value for that given angle.

A close look at Fig. 2(d) shows shifts in the normalized SFG spectral peak position between incidence angles of 42.2° and 42.4°, which corresponds to plasmon coupling range of the FW, confirmed by the minimum in the reflected FW in Fig. 2(b). We calculate the sensitivity for two incident angles within this range for $\varepsilon_3 = 1$ (air). We chose $\theta = 42.35^\circ$, where there is a linear blue shift in the spectrum and $\theta = 42.66^\circ$, where we have a switch in the SFG spectrum which is

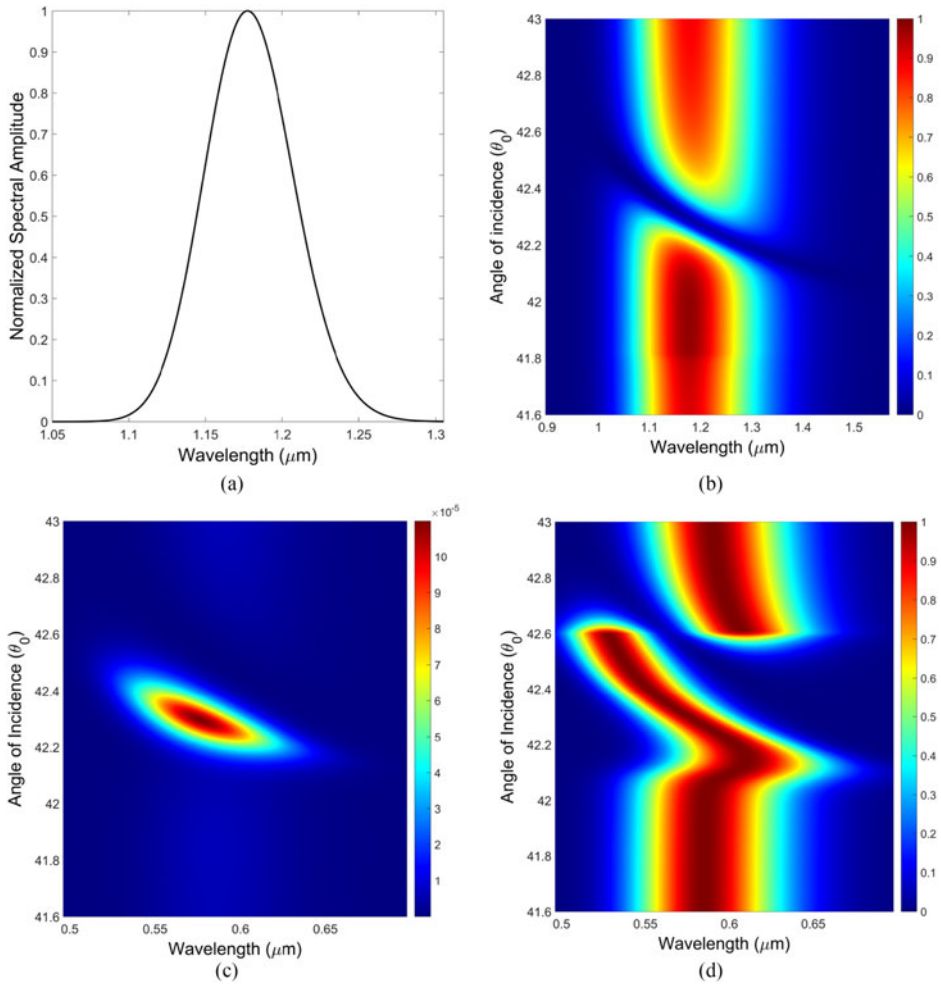

Fig. 2. Far-field spectra of (a) incident FW (b) reflected fundamental spectrum from gold film (c) reflected SFG (d) normalized SFG spectrum. Incident pulse duration is $t_p = 10$ fs.

qualitatively similar to that observed in the Fraunhofer diffraction of light from a circular aperture [44].

Fig. 3(a) and Fig. 3(b) show the shifts in the SFG spectrum with changes in the refractive index n_3(air) at $\theta = 42.35^\circ$ and $\theta = 42.66^\circ$ respectively. We use Eq. (8) and Eq. (9) together with the plots to calculate the sensitivity and the FOM. The proposed sensor can also be used for biological and chemical sensing in solution and therefore the knowledge of its sensitivity in water is desired. We use the wavelength dependent permittivity of water from [45] in our calculations.

The shifts in the SFG spectrum as a result of changing the refractive index of the sample n_3(water) at $\theta = 63.60^\circ$ (linear shift) and $\theta = 64.04^\circ$ (spectral switch) are shown in Fig. 3(c) and Fig. 3(d) respectively. These spectral plots are used to calculate the sensitivity and FOM of the sensor for water solution samples. A comparison of the sensitivity and FOM of both linear and SFG Kretschmann-based sensor modalities in both air and water is presented in Table 1. It should be noted that the measurement range in the linear shift region is not limited to $\Delta n = 0.003 n_3$ and can be extended to $\Delta n = 0.01 n_3$, which is comparable to the sensing range of most linear plasmonic sensors [46]. The narrow measurement range in the region where we have a spectral switch in our sensor could be very useful in sensing samples that undergo very small refractive index changes.

We can infer from Table 1 that both the sensitivity and FOM increase by an order of magnitude in either air or water when we employ an SFG-based versus linear sensor modality. Finally, we observe

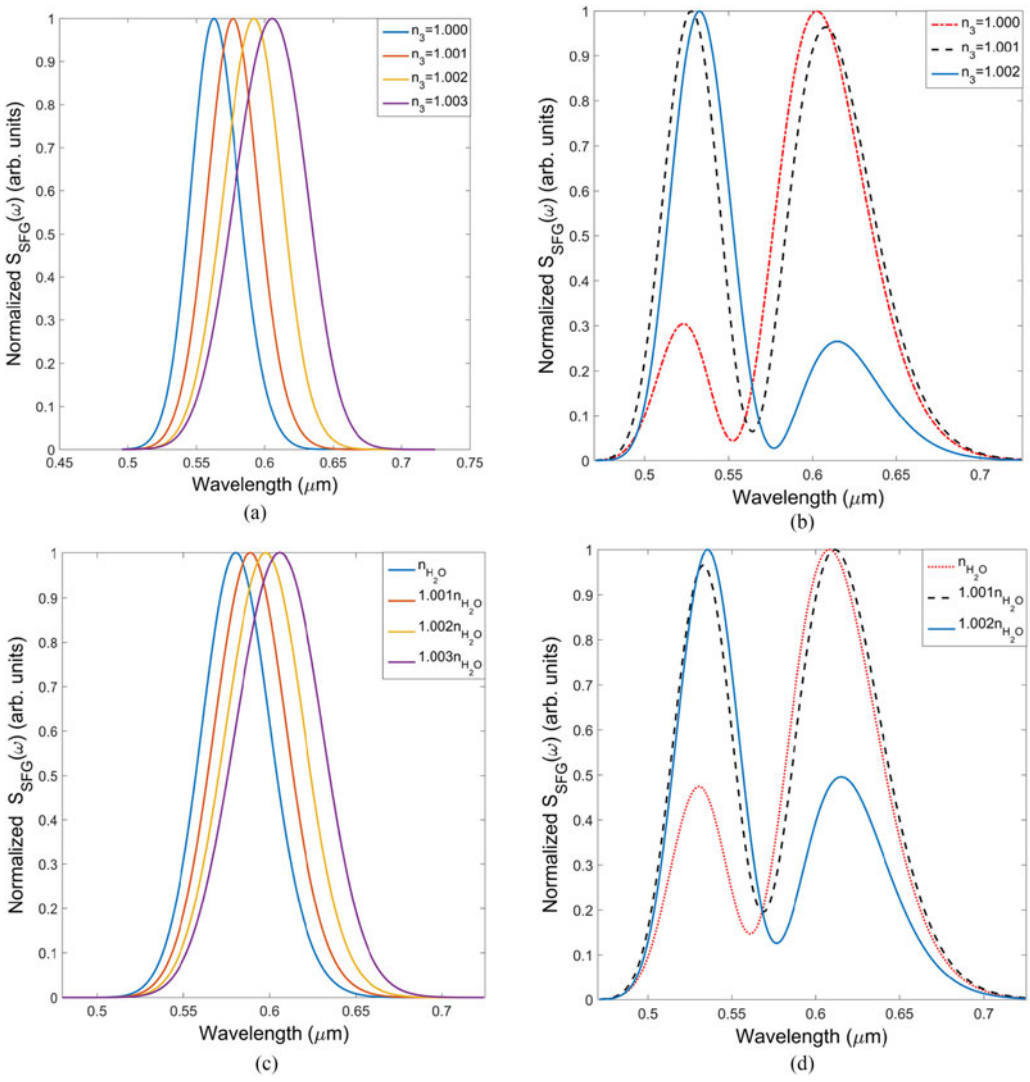

Fig. 3. Reflected far-field SFG spectrum at (a) $\theta = 42.35^\circ$ in air ($S(\lambda) = 14000$ nm/RIU, $FOM = 222$ RIU^{-1}) (b) $\theta = 42.66^\circ$ in air ($S(\lambda) = 35000$ nm/RIU, $FOM = 583$ RIU^{-1}) (c) $\theta = 63.60^\circ$ in water ($S(\lambda) = 6400$ nm/RIU, $FOM = 107$ RIU^{-1}) (d) $\theta = 64.04^\circ$ in water ($S(\lambda) = 28000$ nm/RIU, $FOM = 467$ RIU^{-1}). The incident pulse duration is $t_p = 10$ fs.

TABLE 1
Comparison of Sensitivity and FOM Values of Linear and SFG Kretschmann-Based Sensors in Air and Water

	Linear (588 nm)	SFG (588 nm)
$S_{air}(\lambda)$(nm/RIU)	2600	14000–35000
$S_{water}(\lambda)$(nm/RIU)	1000	6400–28000
FOM_{air}(RIU^{-1})	22	467–583
FOM_{water}(RIU^{-1})	16	107–222

a decrease in both the sensitivity and FOM of both linear and nonlinear sensors in water compared to their operation in air. The analytical expression for sensitivity with wavelength modulation of a Kretschmann-based plasmonic sensor is given by [47]

$$S(\lambda) = \frac{\varepsilon_2^2(\omega)}{\frac{1}{2} \cdot |\frac{d\varepsilon_2(\omega)}{d\lambda}| \cdot n_3^3 + \frac{\varepsilon_2(\omega) n_3}{n_p} \cdot \frac{dn_1}{d\lambda} \cdot (\varepsilon_2^2(\omega) + n_3^2)}. \quad (12)$$

Eq. (12) shows that the sensitivity of a linear Kretschmann-based plasmonic sensor decreases with increase refractive index of the sensing medium. Since the operation of our nonlinear plasmonic sensor is fundamentally based on the principle of the linear Kretschmann sensor through the nonlinear interaction of plasmon-enhanced fundamental waves, we also expect the sensitivity of our nonlinear sensor to decrease with increasing refractive index of the sensing medium. The FOM is defined in terms of the sensitivity and we expect a decrease in sensitivity to be matched with a decrease in the FOM.

4. DFG-Based Sensor

The mid-infrared range is very useful for sensing organic and inorganic molecules [48]. To generate nonlinear signals in this range, we use a dual-wavelength Gaussian pulse and the nonlinear process of DFG. Laser sources with dual wavelengths have been used experimentally to generate sum-frequency waves (SFW) and difference-frequency waves (DFW) in bulk crystals [49]–[53], which demonstrates the potential use of such sources to generate new frequencies in plasmonic materials.

We use a dual-wavelength pulse with peaks at 660 nm ($\omega = 2.854 \times 10^{15}$ rads/s) and 780 nm ($\omega = 2.415 \times 10^{15}$ rads/s), each with a pulse duration of 20 fs. The FW and reflected linear spectrum from the sensor are depicted in Fig. 4(a) and Fig. 4(b), respectively. The reflected linear spectrum has holes corresponding to the surface plasmon coupling angle for each peak wavelength. Using Eq. (1), we obtain $\theta_{spp} = 43.86^\circ$ and $\theta_{spp} = 42.97^\circ$ for the peaks at 660 nm and 780 nm, respectively, which agrees well with the minimum angle positions in Fig. 4(b). The difference-frequency spectrum is shown in Fig. 4(c), with the peak frequency $\omega = 4.39 \times 10^{14}$ rads/s (4.29 μm) corresponding to the difference between the frequency peaks in the FW. The normalized reflected difference-frequency spectrum is shown in Fig. 4(d).

Similarly to the SFG sensor, we use the normalized difference-frequency spectra [see Fig. 4(d)] to estimate the angular region where the sensor is spectrally sensitive. For angles in the range $\theta_0 = 42.7^\circ - 42.9^\circ$, we have a giant spectral switch in the spectrum. For $\theta_0 = 42.9^\circ - 43.39^\circ$, we observe a red shift in the spectrum and finally a blue shift in the spectrum for $\theta_0 = 43.40^\circ - 43.59^\circ$. We proceed to calculate the sensitivity and FOM of our sensor in each of these regions using a representative angle of incidence for both air and water.

Fig. 5 shows the dependence of spectral shifts at the peak DFG wavelength on refractive index change (n_3) in both air and water for different representative angles in the plasmon resonance range of the FW. We use these spectral shift plots to calculate the sensitivity and FOM based on Eq. (8) and Eq. (9). The Kretschmann-based sensor cannot be used in the MIR as a linear sensor due to the large metal losses at these frequencies. Since we cannot compare the performance of our DFG sensor to a linear Kretschmann-based sensor in this range, we have used the sensitivity and FOM values of a recently proposed high sensitivity linear MIR sensor based on metallic nanostructures [54] for comparison. A comparison of the sensitivity and FOM of both linear and nonlinear sensor modalities is presented in Table 2.

The sensitivity of our DFG Kretschmann-based sensor in both air and water is three orders of magnitude higher than that presented in Nguyen-Huu *et al.* [54]. As a result of the high sensitivity values of the DFG sensor, the FOM is almost two orders of magnitude higher than those of the linear sensor. As was the case with the SFG nonlinear sensor, the values of the sensitivity and FOM in water are about half those measured in air.

Nonlinear signals are very difficult to detect due to very small magnitudes of metal nonlinear susceptibilities. It is therefore imperative that we estimate the optical power of the reflected SFG/DFG

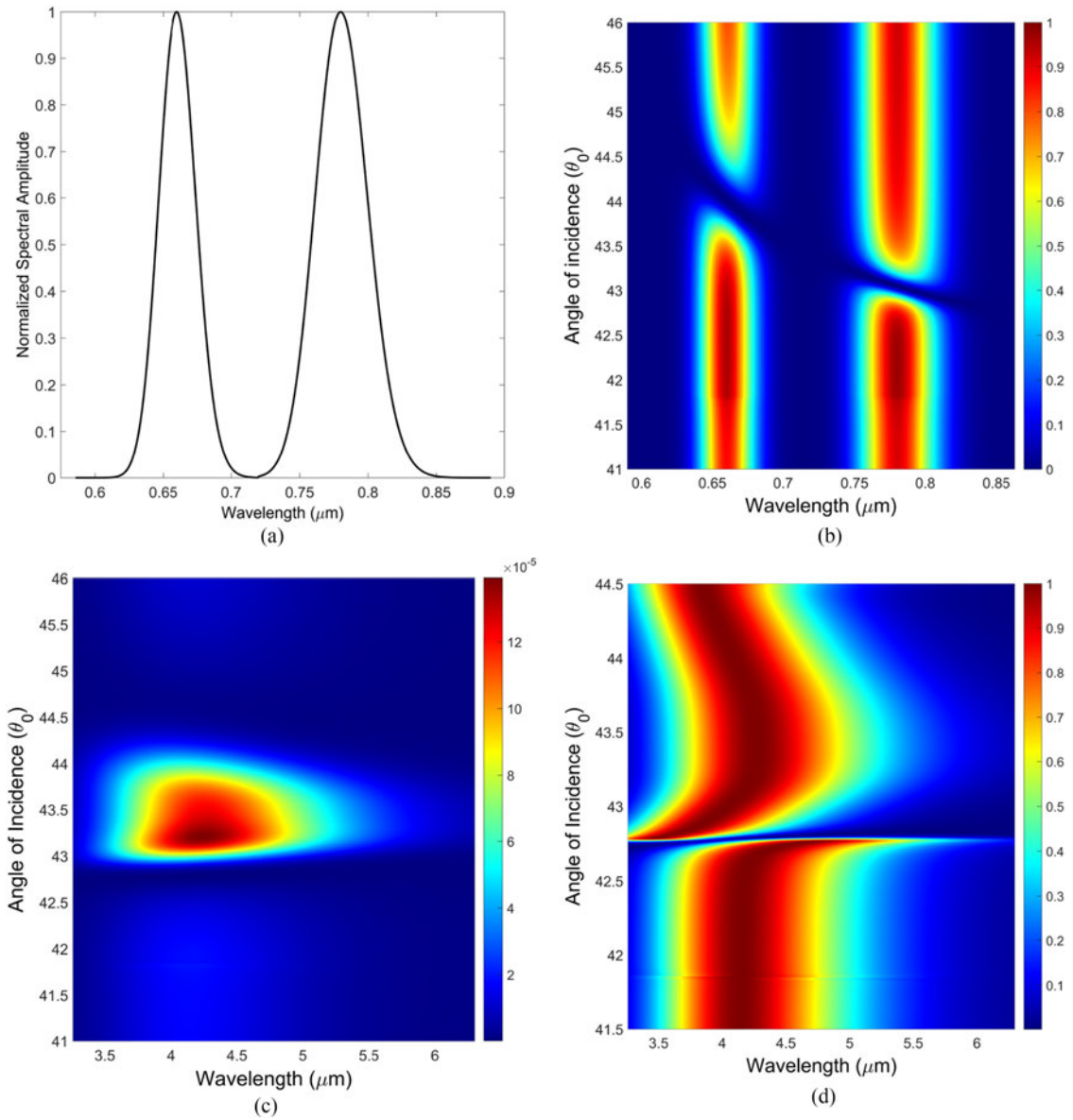

Fig. 4. Far-field spectra of (a) incident FW (b) the reflected fundamental spectrum from gold film (c) reflected DFW (d) normalized DFW. The incident pulse duration is $t_p = 20$ fs.

field to make sure they can be easily detected in order to take advantage of the very high sensitivity values of our sensor. To do this, we assume an incident pulse in both cases has an input power of 100 mW, which is quite reasonable for most femtosecond laser sources. The attenuation from optical elements such as collimators, dichroic mirrors, polarizers, microscope objectives etc., which, incidentally, were all used in a recent study of reflected SHG from conducting thin films [55], was estimated to be 40%. Therefore the power of the source just before incidence on the sample is around 60 mW. From Fig. 2(c) and Fig. 4(c), we observe the power of the reflected nonlinear field to be approximately 10^{-6} times the incident power, thereby leaving us with 60 nW of power immediately after reflection from the sample. Since the reflected fields have to go through optical elements before detection, and assuming a combined attenuation of 40%, this results in a detectable signal of 36 nW. This estimate gives us a reasonable signal power level, which commercial spectrometers such as the Ocean optics USB400, can easily detect. Finally, nonlinear optical measurements from

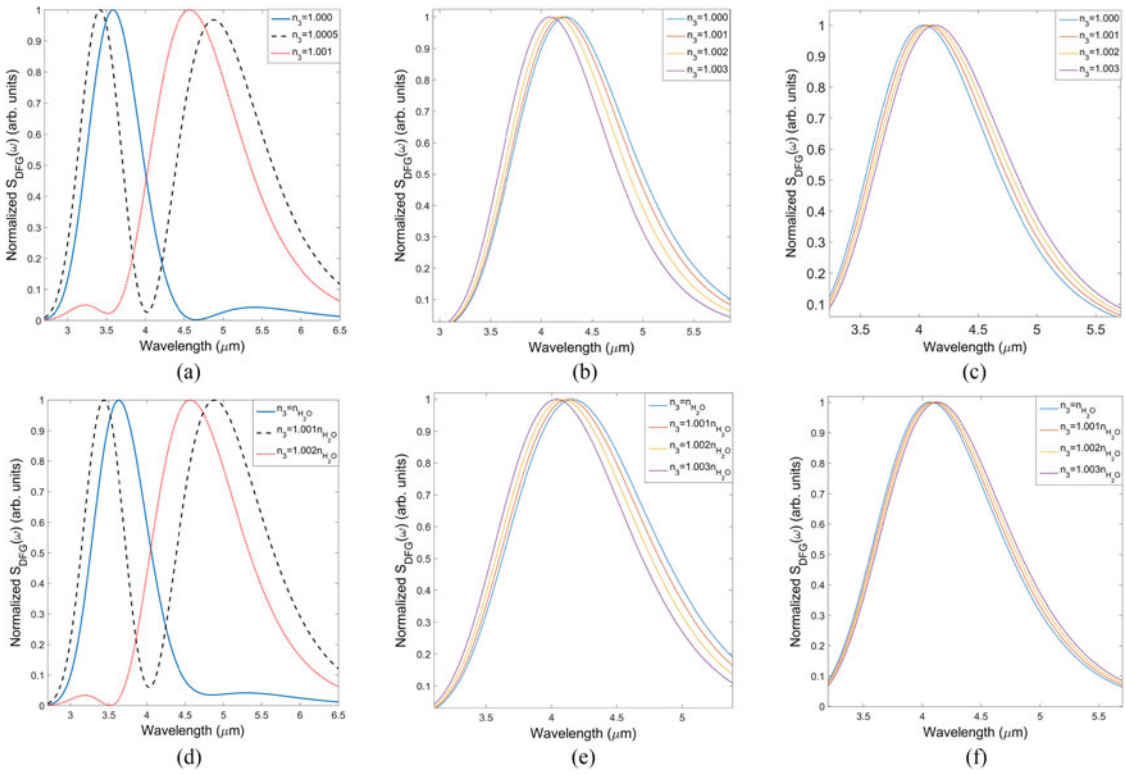

Fig. 5. DFG spectral peak dependence on refractive index n_3 at (a) $\theta_0 = 42.8^\circ$ in air ($S(\lambda) = 1 \times 10^6$ nm/RIU, $FOM = 765$ RIU^{-1}) (b) $\theta_0 = 43.20^\circ$ in air ($S(\lambda) = 5 \times 10^4$ nm/RIU, $FOM = 40$ RIU^{-1}) (c) $\theta_0 = 44.00^\circ$ in air ($S(\lambda) = 3.2 \times 10^4$ nm/RIU, $FOM = 27$ RIU^{-1}) (d) $\theta_0 = 65.81^\circ$ in water ($S(\lambda) = 3.6 \times 10^5$ nm/RIU, $FOM = 300$ RIU^{-1}) (e) $\theta_0 = 66.90^\circ$ in water ($S(\lambda) = 3 \times 10^4$ nm/RIU, $FOM = 23$ RIU^{-1}) (f) $\theta_0 = 71.00^\circ$ in water ($S(\lambda) = 2 \times 10^4$ nm/RIU, FOM = 16 RIU^{-1}). The incident pulse duration is $t_p = 20$ fs.

TABLE 2
Comparison of Sensitivity and FOM Values of Linear and SFG Kretschmann-Based Sensors in Air and Water

	Linear sensor [54]	DFG (4.29 μm)
$S_{air}(\lambda)$(nm/RIU)	8000	3.2×10^4–1.0×10^6
$S_{water}(\lambda)$(nm/RIU)	950	2.0×10^4–3.6×10^5
FOM_{air}(RIU^{-1})	10.26	27–765
FOM_{water}(RIU^{-1})	1.76	16–300

[55] for an incident optical power of 38 mW generated reflected nonlinear signals with a high SNR, which bodes well for our proposed sensor.

Our results also indicate that both the sensitivity and FOM strongly depend on the angle of incidence of the FW. Thus accurate control of the incidence angle is very important for the realization of this sensor. Such control can be achieved by using a goniometer, such as the WT-120 High Precision Motorized goniometer from PI GmbH, which has a resolution of 0.0001°. With such precision, we can accurately control our incident angle.

5. Conclusion

We have proposed the geometry and calculated the sensitivity and FOM of a Kretschmann-based nonlinear plasmonic sensor, operating at both visible and MIR wavelengths through the SFG and DFG nonlinear processes. We demonstrated at specific angles of incidence close to surface plasmon resonance of the FW very high sensitivity values of 1×10^6 nm/RIU and 3.5×10^4 nm/RIU for the DFG and SFG processes respectively in air. Our maximum sensitivity value is three orders of magnitude higher than the wavelength sensitivity of a traditional linear Kretschmann-based sensor. The maximum FOM values of 583 RIU^{-1} and 765 RIU^{-1} for reflected SFG and DFG are an order of magnitude higher than the values typical of a traditional Kretschmann sensor. The maximum sensitivity value for measurements in water, which is highly relevant for biosensing applications, was also three orders of magnitude higher than that of a traditional Kretschmann sensor, making the proposed sensor especially suitable for biological or chemical sensing. Besides the large values of the calculated sensitivity, the proposed sensor gives us the unique ability to operate a Kretschmann-based plasmonic sensor in the MIR, which is otherwise impossible to do in the linear regime. An estimation of the nonlinear signal power from the sensor showed that the nonlinear signal could be easily detected with commercially available spectrometers. We have used a well known geometry, which is very easy to fabricate, and effectively transformed it into an extremely sensitive, versatile surface plasmon sensor using its nonlinear optical properties alone.

References

[1] H. Raether, *Surface Plasmons on Smooth Surfaces*. New York, NY, USA: Springer-Verlag, 1988.
[2] S. A. Maier, *Plasmonics: Fundamentals and Applications*. New York, NY, USA: Springer-Verlag, 2007.
[3] W. L. Barnes, A. Dereux, and T. W. Ebbesen, "Surface plasmon subwavelength optics," *Nature*, vol. 424, no. 6950, pp. 824–830, 2003.
[4] J. Homola, "Surface plasmon resonance sensors for detection of chemical and biological species," *Chem. Rev.*, vol. 108, no. 2, pp. 462–493, 2008.
[5] K. M. Mayer *et al.*, "A label-free immunoassay based upon localized surface plasmon resonance of gold nanorods," *ACS Nano*, vol. 2, no. 4, pp. 687–692, 2008.
[6] S. Lee, K. M. Mayer, and J. H. Hafner, "Improved localized surface plasmon resonance immunoassay with gold bipyramid substrates," *Analytical Chem.*, vol. 81, no. 11, pp. 4450–4455, 2009.
[7] C.-S. Cheng, Y.-Q. Chen, and C.-J. Lu, "Organic vapour sensing using localized surface plasmon resonance spectrum of metallic nanoparticles self assemble monolayer," *Talanta*, vol. 73, no. 2, pp. 358–365, 2007.
[8] K.-J. Chen and C.-J. Lu, "A vapor sensor array using multiple localized surface plasmon resonance bands in a single uv–vis spectrum," *Talanta*, vol. 81, no. 4, pp. 1670–1675, 2010.
[9] E. Kretschmann and H. Raether, "Notizen: Radiative decay of non radiative surface plasmons excited by light," *Zeitschrift für Naturforschung A*, vol. 23, no. 12, pp. 2135–2136, 1968.
[10] S. Roh, T. Chung, and B. Lee, "Overview of the characteristics of micro-and nano-structured surface plasmon resonance sensors," *Sensors*, vol. 11, no. 2, pp. 1565–1588, 2011.
[11] B. Špačková, P. Wrobel, M. Bocková, and J. Homola, "Optical biosensors based on plasmonic nanostructures: A review," *Proc. IEEE*, vol. 104, no. 12, pp. 2380–2408, Dec. 2016.
[12] M. Sun *et al.*, "Integrated plasmonic refractive index sensor based on grating/metal film resonant structure," *Proc. SPIE*, vol, 9757, 2016, Art. no. 97 570Q.
[13] A. González-Cano, M.-C. Navarrete, Ó. Esteban, and N. Díaz-Herrera, "Plasmonic sensors based on doubly-deposited tapered optical fibers," *Sensors*, vol. 14, no. 3, pp. 4791–4805, 2014.
[14] J. Burgmeier, A. Feizpour, W. Schade, and B. M. Reinhard, "Plasmonic nanoshell functionalized etched fiber bragg gratings for highly sensitive refractive index measurements," *Opt. Lett.*, vol. 40, no. 4, pp. 546–549, 2015.
[15] M. Lippitz, M. A. van Dijk, and M. Orrit, "Third-harmonic generation from single gold nanoparticles," *Nano Lett.*, vol. 5, no. 4, pp. 799–802, 2005.
[16] S. Palomba, H. Harutyunyan, J. Renger, R. Quidant, N. F. van Hulst, and L. Novotny, "Nonlinear plasmonics at planar metal surfaces," *Philosophical Trans. Roy. Soc. London A, Math., Phys. Eng. Sci,*, vol. 369, no. 1950, pp. 3497–3509, 2011.
[17] T. Utikal *et al.*, "Towards the origin of the nonlinear response in hybrid plasmonic systems," *Phys. Rev. Lett.*, vol. 106, no. 13, 2011, Art. no. 133901.
[18] H. Harutyunyan, G. Volpe, R. Quidant, and L. Novotny, "Enhancing the nonlinear optical response using multifrequency gold-nanowire antennas," *Phys. Rev. Lett.*, vol. 108, no. 21, 2012, Art. no. 217403.
[19] M. Kauranen and A. V. Zayats, "Nonlinear plasmonics," *Nature Photon.*, vol. 6, no. 11, pp. 737–748, 2012.
[20] M. Ciappina, S. S. Aćimović, T. Shaaran, J. Biegert, R. Quidant, and M. Lewenstein, "Enhancement of high harmonic generation by confining electron motion in plasmonic nanostrutures," *Opt. Exp.*, vol. 20, no. 24, pp. 26 261–26 274, 2012.

[21] A. K. Singh *et al.*, "Gold nanorod based selective identification of escherichia coli bacteria using two-photon rayleigh scattering spectroscopy," *ACS Nano*, vol. 3, no. 7, pp. 1906–1912, 2009.
[22] A. Neely *et al.*, "Ultrasensitive and highly selective detection of alzheimers disease biomarker using two-photon rayleigh scattering properties of gold nanoparticle," *ACS Nano*, vol. 3, no. 9, pp. 2834–2840, 2009.
[23] M. Mesch, B. Metzger, M. Hentschel, and H. Giessen, "Nonlinear plasmonic sensing," *Nano Lett.*, vol. 16, no. 5, pp. 3155–3159, 2016.
[24] L. Wang, F. Che, S. A. Ponomarenko, and Z. D. Chen, "Plasmon-enhanced spectral changes in surface sum-frequency generation with polychromatic light," *Opt. Exp.*, vol. 21, no. 12, pp. 14 159–14 168, 2013.
[25] F. Che, S. A. Ponomarenko, and M. Cada, "Giant spectral transformations in plasmon-enhanced difference-frequency generation with polychromatic light," *J. Opt.*, vol. 18, no. 12, 2016, Art. no. 125503.
[26] B. H. Ong, X. Yuan, S. C. Tjin, J. Zhang, and H. M. Ng, "Optimised film thickness for maximum evanescent field enhancement of a bimetallic film surface plasmon resonance biosensor," *Sens.Actuators B, Chem.*, vol. 114, no. 2, pp. 1028–1034, 2006.
[27] Q.-H. Phan, N. Nguyen-Huu, and Y.-L. Lo, "Optimized double-layered grating structures for chem/biosensing in midinfrared range," *IEEE Sensors J.*, vol. 14, no. 9, pp. 2938–2946, Sep. 2014.
[28] L. Mandel and E. Wolf, *Optical Coherence and Quantum Optics*. Cambridge, U.K.: Cambridge Univ. Press, 1995.
[29] S. A. Ponomarenko, H. Roychowdhury, and E. Wolf, "Physical significance of complete spatial coherence of optical fields," *Phys. Lett. A*, vol. 345, no. 1-3, pp. 10–12, 2005.
[30] S. A. Ponomarenko and E. Wolf, "The spectral degree of coherence of fully spatially coherent electromagnetic beams," *Opt. Commun.*, vol. 227, no. 1, pp. 73–74, 2003.
[31] P. Yeh, *Optical Waves in Layered Media* (Series in Pure and Applied Optics). Hoboken, NJ, USA: Wiley, 1998.
[32] W. C. Chew, *Waves and Fields in Inhomogeneous Media,*, 2nd ed. New York, NY, USA: Inst. Elect.Electron. Eng., 1995.
[33] S. A. Ponomarenko, G. P. Agrawal, and E. Wolf, "Energy spectrum of a nonstationary ensemble of pulses," *Opt. Lett.*, vol. 29, no. 4, pp. 394–396, 2004.
[34] R. W. Boyd, *Nonlinear Optics*, 2nd ed. Boston, MA, USA: Academic, 2003.
[35] L. Novotny and B. Hecht, *Principles of Nano-Optics*. Cambridge, U.K: Cambridge Univ. Press, 2006.
[36] J. Homola, I. Koudela, and S. S. Yee, "Surface plasmon resonance sensors based on diffraction gratings and prism couplers: Sensitivity comparison," *Sens. Actuators B, Chem.*, vol. 54, no. 1, pp. 16–24, 1999.
[37] Z. Chen, X. Zhao, C. Lin, S. Chen, L. Yin, and Y. Ding, "Figure of merit enhancement of surface plasmon resonance sensors using absentee layer," *Appl. Opt.*, vol. 55, no. 25, pp. 6832–6835, 2016.
[38] N. Cennamo, D. Massarotti, L. Conte, and L. Zeni, "Low cost sensors based on SPR in a plastic optical fiber for biosensor implementation," *Sensors*, vol. 11, no. 12, pp. 11 752–11 760, 2011.
[39] J. Homola, "Electromagnetic theory of surface plasmons," in *Surface Plasmon Resonance Based Sensors*. New York, NY, USA: Springer-Verlag, 2006, pp. 3–44.
[40] Y. Zhong, S. D. Malagari, T. Hamilton, and D. Wasserman, "Review of mid-infrared plasmonic materials," *J. Nanophoton.*, vol. 9, no. 1, 2015, Art. no. 093791.
[41] J. Sambles, G. Bradbery, and F. Yang, "Optical excitation of surface plasmons: An introduction," *Contemporary Phys.*, vol. 32, no. 3, pp. 173–183, 1991.
[42] X. Huang, P. Zhu, X. Liu, Y. Leng, X. Lu, and H. Wang, "Spectral modulation of ultra-broadband femtosecond laser pulses based on surface plasmon resonance," *Opt. Commun.*, vol. 283, no. 11, pp. 2373–2377, 2010.
[43] H. R. Gwon and S. H. Lee, "Spectral and angular responses of surface plasmon resonance based on the kretschmann prism configuration," *Mater. Trans.*, vol. 51, no. 6, pp. 1150–1155, 2010.
[44] S. A. Ponomarenko and E. Wolf, "Spectral anomalies in a fraunhofer diffraction pattern," *Opt. Lett.*, vol. 27, no. 14, pp. 1211–1213, 2002.
[45] M. R. Querry, D. M. Wieliczka, and D. J. Segelstein, "Water (h2o)," in *Handbook of Optical Constants of Solids*, E. D. Palik, Ed. Burlington, MA, USA: Academic, 1997, pp. 1059–1077.
[46] F. Bahrami, M. Maisonneuve, M. Meunier, J. S. Aitchison, and M. Mojahedi, "An improved refractive index sensor based on genetic optimization of plasmon waveguide resonance," *Opt. Exp.*, vol. 21, no. 18, pp. 20 863–20 872, 2013.
[47] A. Shalabney and I. Abdulhalim, "Sensitivity-enhancement methods for surface plasmon sensors," *Laser Photon. Rev.*, vol. 5, no. 4, pp. 571–606, 2011.
[48] C. Fischer and M. W. Sigrist, "Mid-ir difference frequency generation," *Top. Appl. Phys.*, vol. 89, pp. 99–143, 2003.
[49] A. Majki *et al.*, "Terahertz source at 9.4 Thz based on a dual-wavelength infrared laser and quasi-phase matching in organic crystals oh1," *Appl. Phys. Lett.*, vol. 105, no. 14, 2014, Art. no. 141115.
[50] P. Zhao, S. Ragam, Y. J. Ding, and I. B. Zotova, "Compact and portable terahertz source by mixing two frequencies generated simultaneously by a single solid-state laser," *Opt. Lett.*, vol. 35, no. 23, pp. 3979–3981, 2010.
[51] K. Zhong *et al.*, "Compact high-repetition-rate monochromatic terahertz source based on difference frequency generation from a dual-wavelength nd: Yag laser and dast crystal," *J. Infrared, Millim., aThz Waves*, vol. 38, no. 1, pp. 87–95, 2017.
[52] Y. Chang, H. Chang, K. Su, and Y. Chen, "High-efficiency q-switched dual-wavelength emission at 1176 and 559 nm with intracavity raman and sum-frequency generation," *Opt. Exp.*, vol. 17, no. 14, pp. 11 892–11 897, 2009.
[53] P. Zhao, "Compact terahertz sources based on difference frequency generation," Ph.D. dissertation, Dept. Elect. Eng., Lehigh Univ, Bethlehem, PA, 2012.
[54] N. Nguyen-Huu *et al.*, "Mid-infrared fano resonance in heavily doped silicon and metallic nanostructures due to coupling of wood–rayleigh anomaly and surface plasmons," *J. Phys. D, Appl. Phys.*, vol. 50, no. 20, 2017, Art. no. 205105.
[55] F. Che, S. Grabtchak, W. M. Whelan, S. A. Ponomarenko, and M. Cada, "Relative SHG measurements of metal thin films: Gold, silver, aluminum, cobalt, chromium, germanium, nickel, antimony, titanium, titanium nitride, tungsten, zinc, silicon and indium tin oxide," *Results Phys.*, vol. 7, pp. 593–595, 2017.